

Supporting Information for:

Mechanism and Driving Force of NO Transfer from S-Nitrosothiol to Cobalt(II) Porphyrin: a Detailed Thermodynamic and Kinetic Study

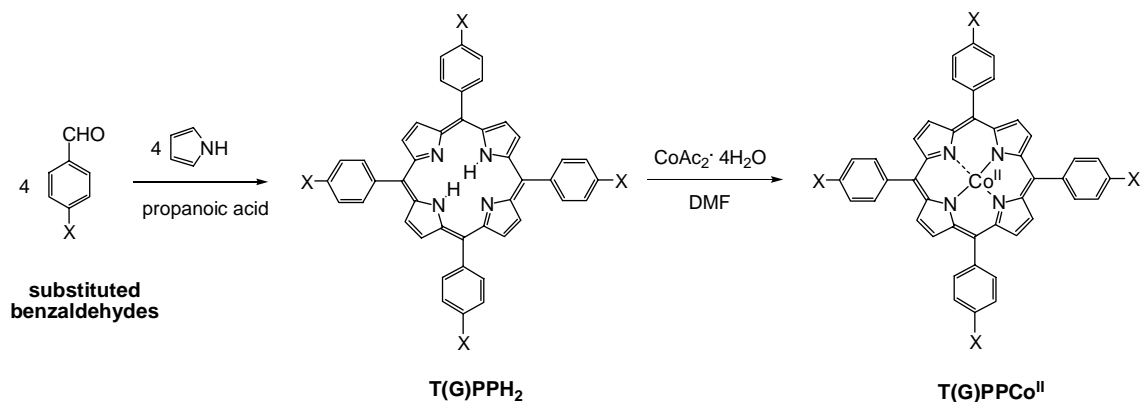
Xiao-Qing Zhu,* Jian-Yu Zhang, and Jin-Pei Cheng*

Department of Chemistry, the State Key Laboratory of Elemento-Organic Chemistry, Nankai University, Tianjin 300071, China

Contents

1) Experimental details	Page S2-S4
2) Estimation of the heterolytic and homolytic S-NO bond dissociation energies of Ph ₃ CSNO.	Page S5-S6
3) The IR and UV-vis spectra of the reactants and products (Figure S3-S5)	Page S7-S9
4) The data fitting of k_{obs} and the derivation of k_2 (Figure S6-S7)	Page S10-S11
5) The Arrhenius plot of $\ln k_2$ versus $1/T$ as well as the Eyring plot of $\ln(k_2/T)$ versus $1/T$ for the reaction of T(G)PPCo ^{II} NO with Ph ₃ CSNO (Figure S8-S13)	Page S12-S17
6) Correlations of $\log k_2$ (at 298 K) versus spin-delocalization parameter $4\sigma_{\text{JJ}}^{\bullet}$ (Figure S14)	Page S18
7) Binary-correlation of $\log k_2$ (at 298 K) versus $(0.76\sigma + 0.07\sigma_{\text{ij}})$ for the NO transfer reaction (Figure S15)	Page S19
8) Plots of $\log k_2$ (at 298 K) against the redox potentials of T(G)PPCo ^{II} , BDEs of T(G)PPCo ^{II} -NO (Figure S16-S17)	Page S20-S21
9) References in Supporting Information	Page S22

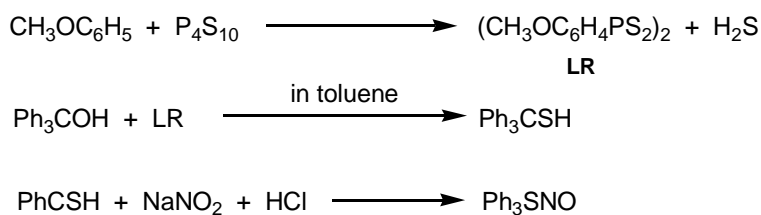
Experimental Details



Scheme S1. Synthesis Route for the $T(G)PPCo^{II}$.

The para- and meta-substituted tetraphenylporphyrin free bases $T(G)PPH_2$, where G = *p*-OCH₃, *p*-CH₃, H, *p*-Cl, *p*-Br, *p*-NO₂, *p*-iPr, *m*-OCH₃, *m*-CH₃, *m*-Cl, *m*-Br, and *m*-NO₂, were synthesized by condensation of the precursor benzaldehydes and pyrrole using the method of Adler et al.^{S1} and chromatographed on silica gel with dichloromethane at least once before use.

The corresponding cobalt derivative, $T(G)PPCo^{II}$, was obtained by refluxing the free-base porphyrins with $Co(CH_3CO_2)_2 \cdot 4H_2O$ in dimethylformamide by the method of Adler et al.^{S2} The products were chromatographed at least three times as described above for $T(G)PPH_2$, the final time using benzene as the solvent. Each time only the center cut was retained.



Scheme S2. Synthesis route of Ph₃CSNO.

The synthesis of LR:^{S3} 108ml of processed anisole was added in four-neck round bottomed flask. Moisture was strictly excluded. After bubbling nitrogen for 15 min, 44.4g of P₄S₁₀ was added. Another 30 min nitrogen bubbling was needed. The mixture was agitated and heated to reflux for 6 h and then cooled to room temperature and filtrated both in nitrogen environment to give the light yellow solid. The product was dried in vacuum and stored in the glove-box.

The synthesis of Triphenylmethanethiol:^{S4} 2.63g triphenylmethanol and 2.02g LR were dissolved in 285 ml processed toluene in Ar environment, stirred and reflux for 20 min. Cool in Ar atmosphere and the solution turn blue. The solvent removed in vacuo to give the crude material. Further purification was taken on by the column chromatography using toluene/petroleum (1:3) as the eluant to give the white product. M.p. 100 ~102 °C.

The synthesis of S-Nitrosotriphenylmethanethiol:^{S5} In a two-phase reaction triphenylmethanethiol (1.16 mmol/20 mL of CH₂Cl₂) was shaken with an 20 ml acidified solution of sodium nitrite (11.6 mmol of NaNO₂ in 5 mL of concentrated hydrochloric acid). A green color rapidly formed. The solution was allowed to stand, the clear aqueous phase was then removed, and the organic layer was washed with NaHCO₃ and water three times, dried in Na₂SO₄ and filtrated. The solvent removed in vacuo to give the green crystals product which was then dried under vacuum.

Spectral Titration

The spectral titration used to determine the reaction stoichiometry proceeded as follows: the concentration of $\text{T(G)PPCo}^{\text{II}}$ is always larger than the concentration of Ph_3CSNO . Different concentration of Ph_3CSNO was added into the solution of $\text{T(G)PPCo}^{\text{II}}$ and the absorption of $\text{T(G)PPCo}^{\text{II}}$ at 415 to 420 nm depending on the substituents of $\text{T(G)PPCo}^{\text{II}}$ was monitored to calculate the consumption of $\text{T(G)PPCo}^{\text{II}}$. Plot of the consumption of $\text{T(G)PPCo}^{\text{II}}$ vs the addition of Ph_3CSNO would give a slope of about 1, meaning the one mole of $\text{T(G)PPCo}^{\text{II}}$ were required to consume one mole of Ph_3CSNO .

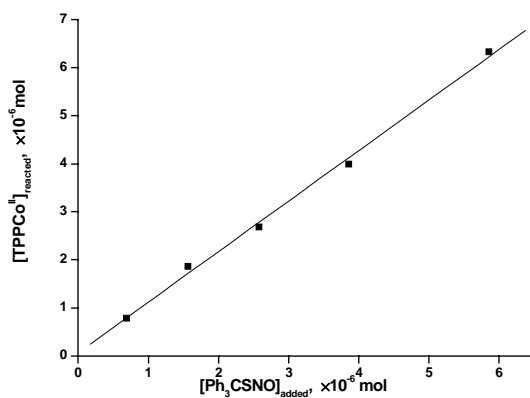
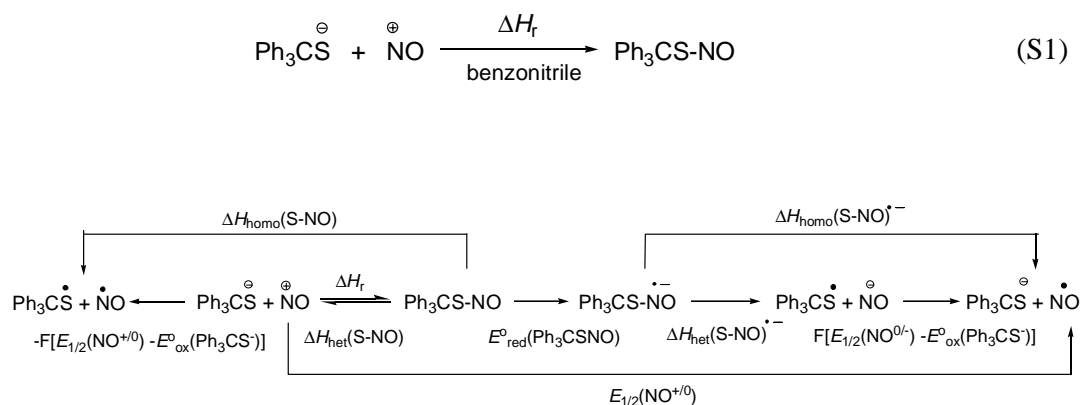


Figure S1. Plot of the consumption of TPPCo^{II} vs the addition of Ph_3CSNO .

Estimation of the Heterolytic and Homolytic S-NO Bond Dissociation Energies of Ph₃CSNO and Its Radical Anion in Benzonitrile. Heterolytic S-NO bond dissociation energy of Ph₃CSNO in benzonitrile [$\Delta H_{\text{het}}(\text{S-NO})$] was obtained from the reaction heat of triphenylmethanethiol anion (Ph₃CS[−]) with NO⁺ cation (NO⁺ClO₄[−]) in dry anaerobic benzonitrile solution (eqs S1 and S2). The reaction heat of Ph₃CS[−] with NO⁺ can be directly determined by titration calorimetry (Figure S2). The homolytic S-NO bond dissociation energy of Ph₃CSNO [$\Delta H_{\text{homo}}(\text{S-NO})$] and the heterolytic and homolytic (S-NO)^{•−} bond dissociation energies of Ph₃CSNO radical anion (Ph₃CSNO^{•−}) in benzonitrile [$\Delta H_{\text{het}}(\text{S-NO})^{\bullet-}$ and $\Delta H_{\text{homo}}(\text{S-NO})^{\bullet-}$] were obtained according to the eqs S2-S6, respectively, which were derived from the suitable thermodynamic cycles as shown in Scheme S1. The results are summarized in Table 4 in the manuscript.



Scheme S1. Thermodynamic cycles on the basis of the reaction of triphenylmethanethiol anion (Ph₃CS[−]) with NO⁺ cation (NO⁺ClO₄[−]).

$$\Delta H_{\text{het}}(\text{S-NO}) = -\Delta H_{\text{r}} \quad (\text{S2})$$

$$\Delta H_{\text{homo}}(\text{S-NO}) = \Delta H_{\text{het}}(\text{S-NO}) - F[E_{1/2}(\text{NO}^{+/0}) - E_{\text{ox}}^{\text{O}}(\text{Ph}_3\text{CS}^{0/-})] \quad (\text{S3})$$

$$\Delta H_{\text{het}}(\text{S-NO})^{\bullet} = \Delta H_{\text{homo}}(\text{S-NO}) + F[E_{\text{red}}^{\text{O}}(\text{Ph}_3\text{CSNO}) - E_{1/2}(\text{NO}^{0/-})] \quad (\text{S4})$$

$$\Delta H_{\text{homo}}(\text{S-NO})^{\bullet} = \Delta H_{\text{het}}(\text{S-NO}) - F[E_{1/2}(\text{NO}^{+/0}) - E_{\text{red}}^{\text{O}}(\text{Ph}_3\text{CSNO})] \quad (\text{S5})$$

$$\Delta G_{\text{et}} = -F[E_{1/2}(\text{NO}^{+/0}) - E_{\text{ox}}^{\text{O}}(\text{Ph}_3\text{CS}^{0/-})] \quad (\text{S6})$$

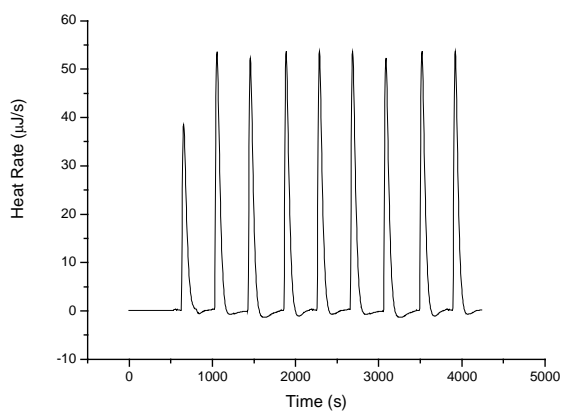
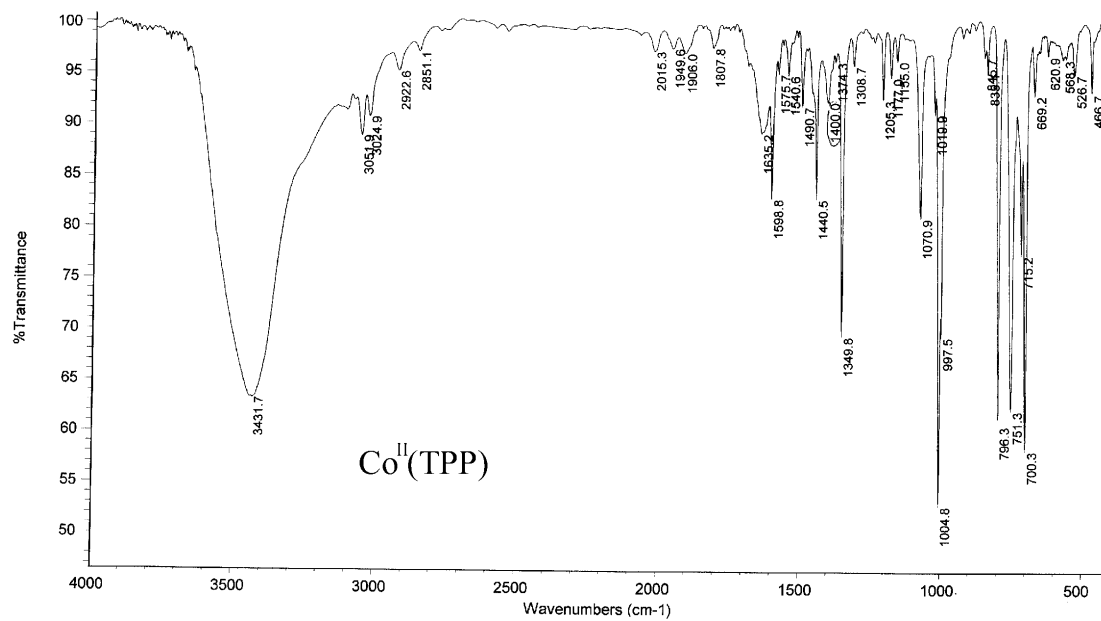
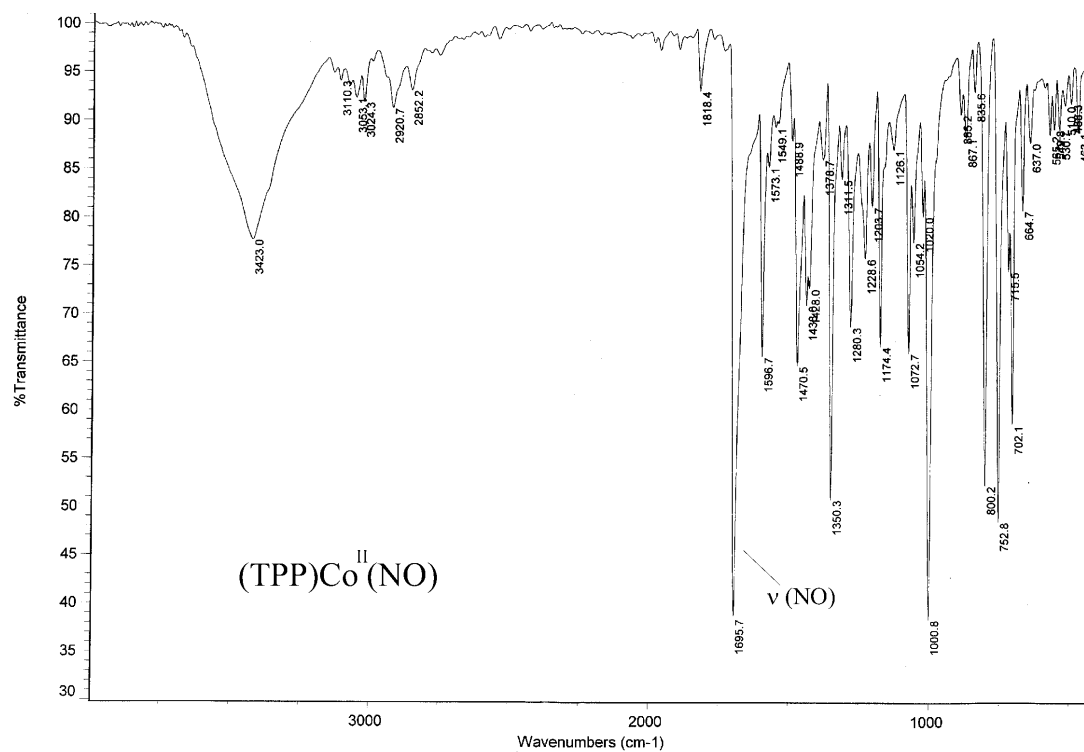


Figure S2. Isothermal titration calorimetry (ITC) for the reaction of $\text{NO}^+\text{ClO}_4^-$ with $\text{Ph}_3\text{CS}^+\text{K}^+$ in benzonitrile at 298 K. Titration was conducted by adding 10 μL of $\text{NO}^+\text{ClO}_4^-$ (0.85 mM) every 400s into the benzonitrile containing $\text{Ph}_3\text{CS}^+\text{K}^+$ (0.47 mM).



(a)



(b)

Figure S3. The IR spectra of T(H)PPCo^{II} (a) and T(H)PPCo^{II}NO (b).

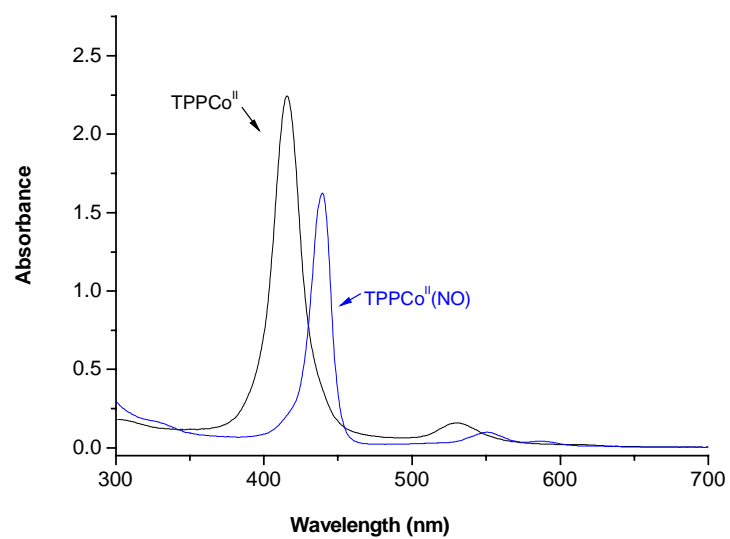


Figure S4. UV-vis spectra of TPPCo^{II} (black line) and TPPCo^{II}NO (blue line) in benzonitrile.

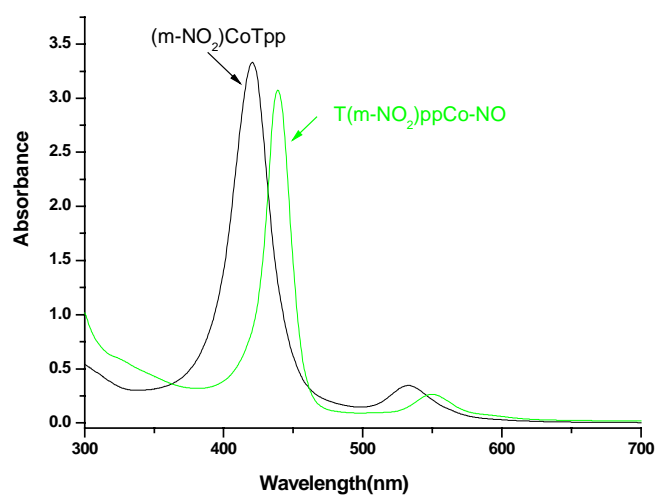


Figure S5. UV-vis spectra of T(m-NO₂)PPCo^{II} (black line) and T(m-NO₂)PPCo^{II}NO (green line) in benzonitrile.

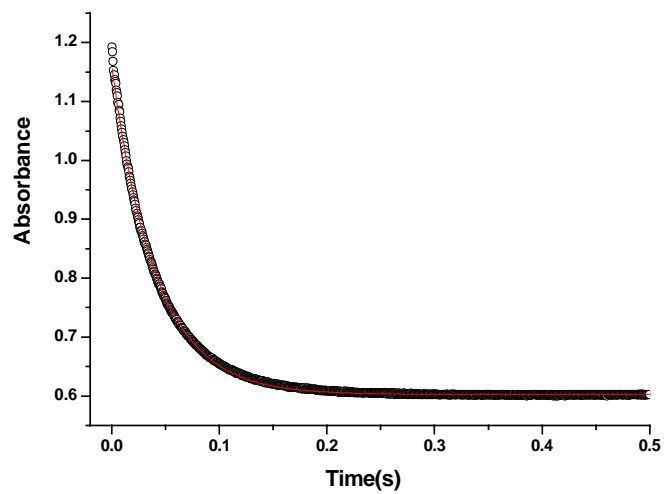


Figure S6. The data fitting for the reaction of $T(m\text{-NO}_2)\text{PPCo}^{\text{II}}$ with Ph_3CSNO under pseudo-first order reaction condition in benzonitrile at 25 °C (black circles for origin data and red line for the fitting).

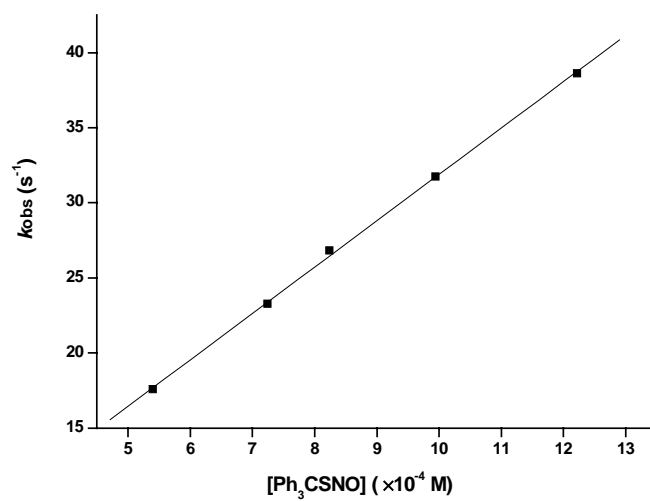


Figure S7. The plot of k_{obs} versus the concentration of Ph_3CSNO for the reaction of $\text{T(H)PPCo}^{\text{II}}$ [$\text{C} = 2.98 \times 10^{-5} \text{ M}$] with Ph_3CSNO under pseudo-first order reaction condition in benzonitrile at 25 °C.

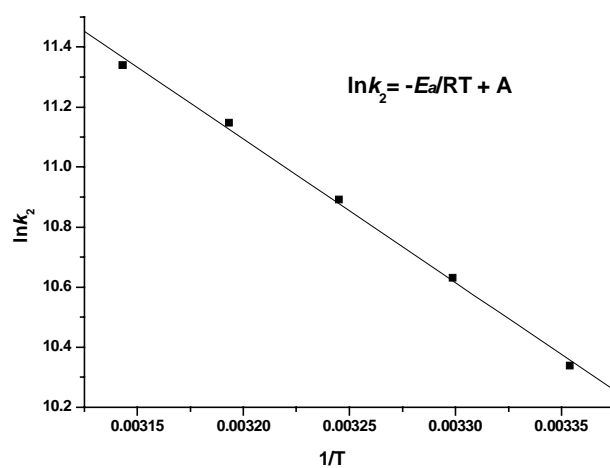


Figure S8. The Arrhenius plot of $\ln k_2$ versus $1/T$ for the reaction of $T(H)PPCo^{II}$ with Ph_3CSNO in benzonitrile.

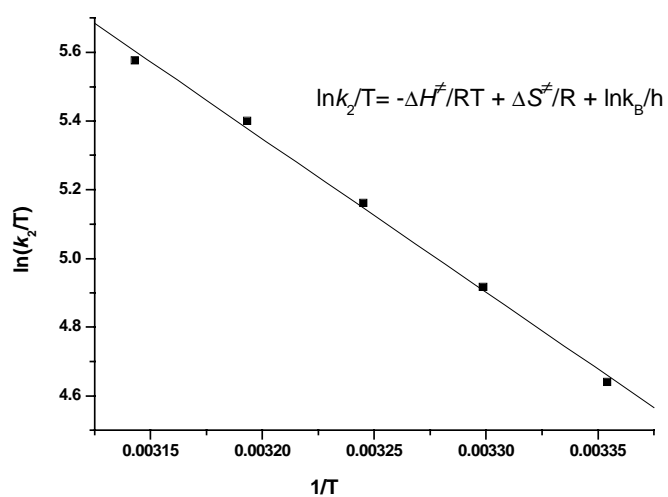


Figure S9. The Eyring plot of $\ln(k_2/T)$ versus $1/T$ for the reaction of T(H)PPCo^{II} with Ph₃CSNO in benzonitrile.

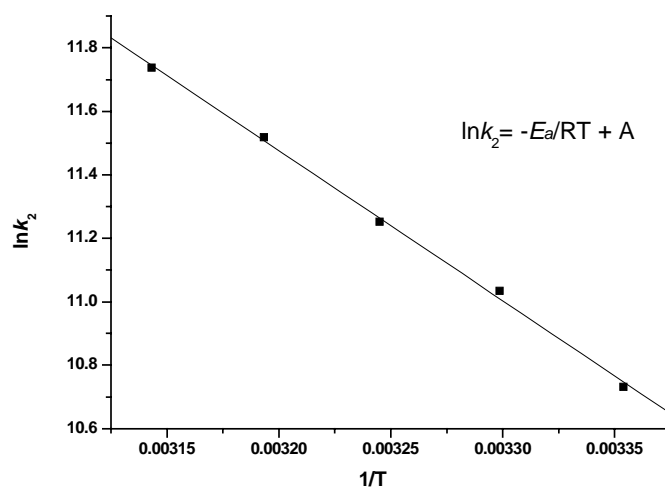


Figure S10. The Arrhenius plot of $\ln k_2$ versus $1/T$ for the reaction of $T(p\text{-OMe})\text{PPCo}^{\text{II}}$ with Ph_3CSNO in benzonitrile.

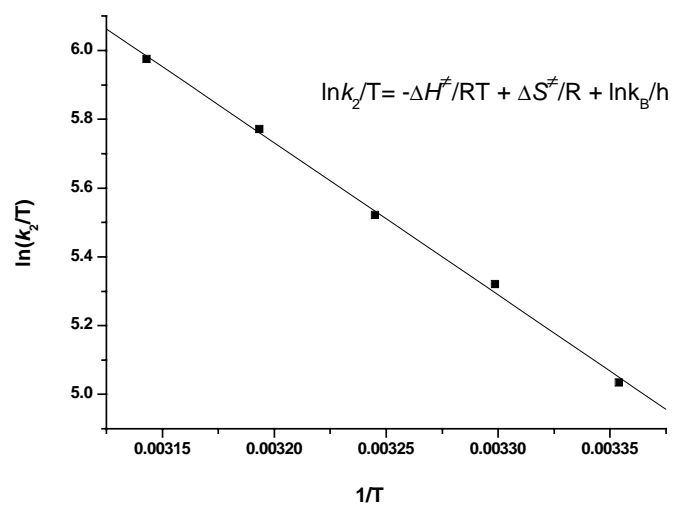


Figure S11. The Eyring plot of $\ln(k_2/T)$ versus $1/T$ for the reaction of $T(p\text{-OMe})\text{PPCo}^{\text{II}}$ with Ph_3CSNO in benzonitrile.

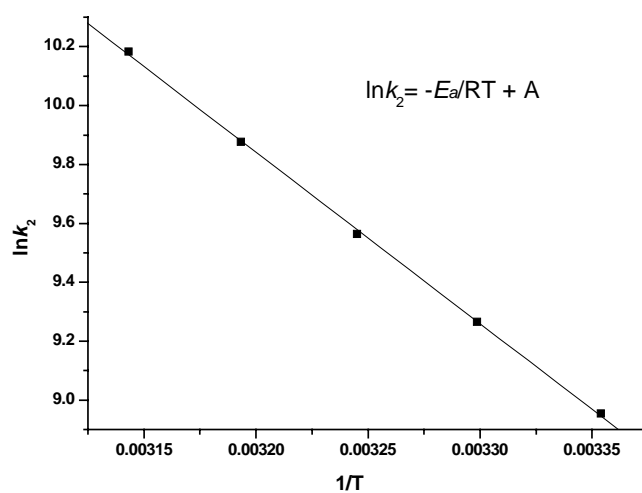


Figure S12. The Arrhenius plot of $\ln k_2$ versus $1/T$ for the reaction of $T(m\text{-NO}_2)\text{PPCo}^{\text{II}}$ with Ph_3CSNO in benzonitrile.

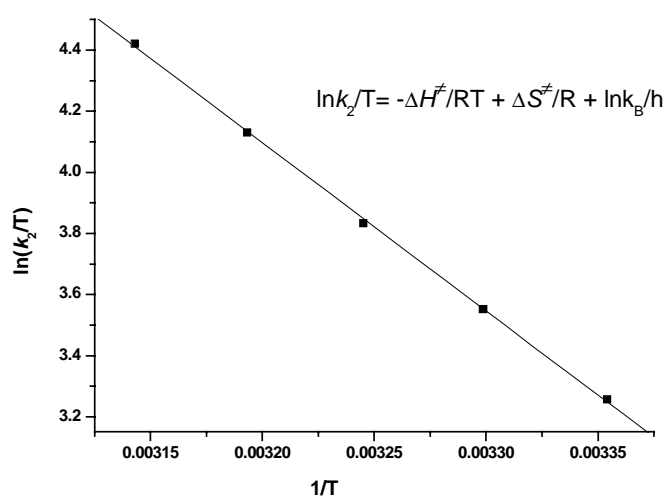


Figure S13. The Eyring plot of $\ln(k_2/T)$ versus $1/T$ for the reaction of $T(m\text{-NO}_2)\text{PPCo}^{\text{II}}$ with Ph_3CSNO in benzonitrile.

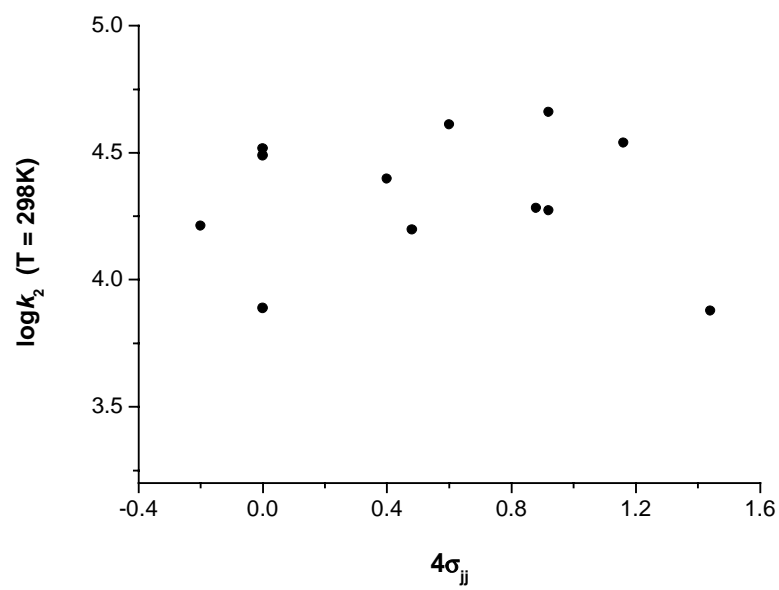


Figure S14. Correlations of $\log k_2$ (at 298 K) versus spin-delocalization parameter $4\sigma_{JJ}^\bullet$ the reactions of Ph_3CSNO with $\text{T(G)PPCo}^{\text{II}}$ in benzonitrile.

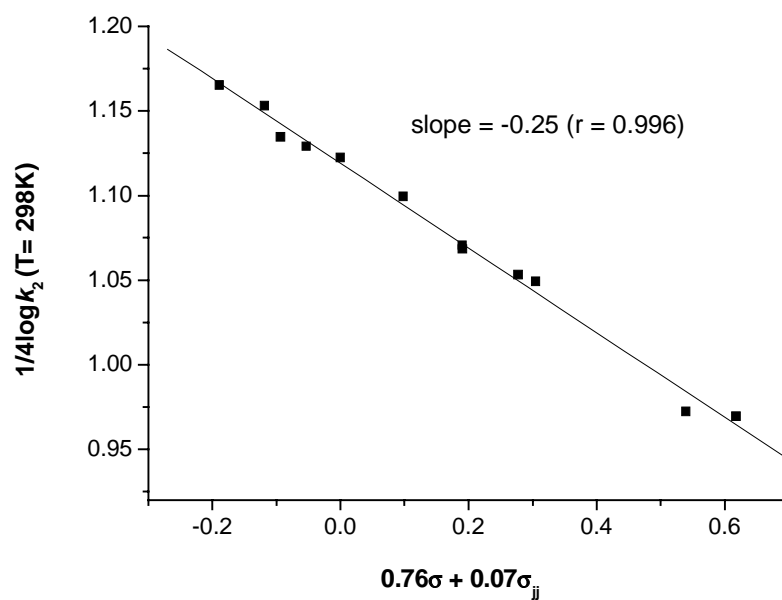


Figure S15. Binary-correlation of $\log k_2$ (at 298 K) versus $(0.76\sigma + 0.07\sigma_{ij})$ for the reactions of Ph_3CSNO with $\text{T(G)PPCo}^{\text{II}}$ in benzonitrile.

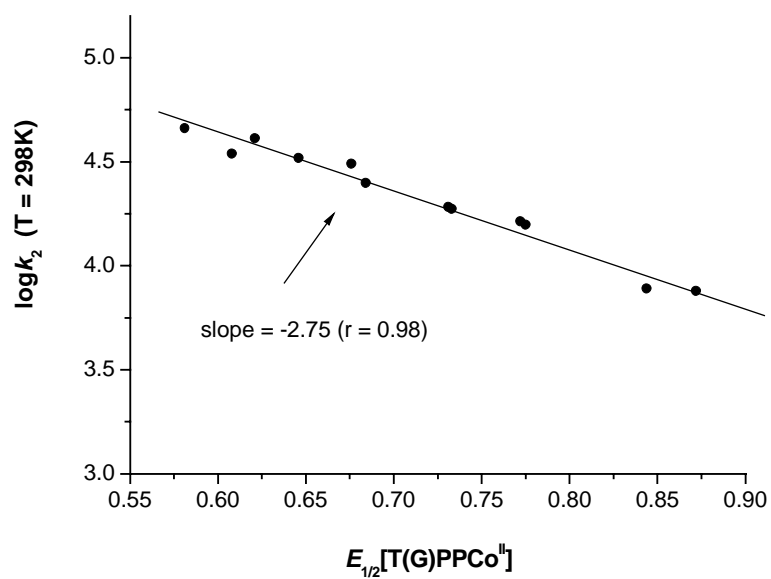


Figure S16. Plots of $\log k_2$ (at 298 K) against the redox potentials of T(G)PPCo^{II} for the reactions of Ph₃CSNO with T(G)PPCo^{II} in benzonitrile.

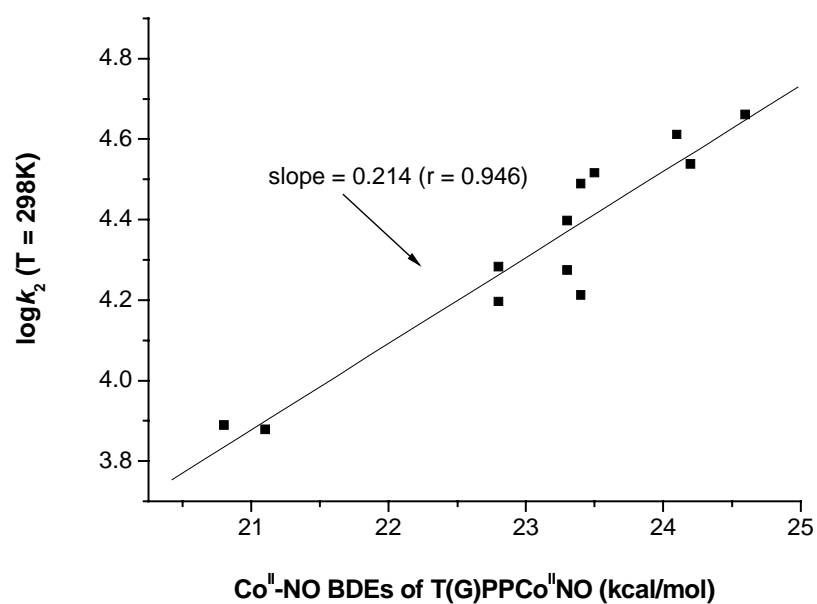


Figure S17. Plots of $\log k_2$ (at 298 K) for the reactions of Ph_3CSNO with $\text{T(G)PPCo}^{\text{II}}$ against the BDEs of $\text{Co}^{\text{II}}\text{-NO}$ bond in $\text{T(G)PPCo}^{\text{II}}\text{-NO}$.

References in Supporting Information:

- (S1) Alder, A. D.; Longo, F. R.; Finarelli, J. D.; Goldmacher, J.; Assour, J.; Korsakoff, L. *J. Org. Chem.* **1967**, *32*, 476.
- (S2) Adler, A. D.; Longo, F. R. Kampas, F.; Kim, J. *J. Inorg. Nucl. Chem.* **1970**, *32*, 2443.
- (S3) Lecher, H. Z.; Greenwood, R. A.; Whitehouse, K. C.; Chao, T. H. *J. Am. Chem. Soc.* **1956**, *78*, 5018-5022.
- (S4) Nishio, T. *J. Chem. Soc., Perkin Trans. I* **1993**, 1113-1117.
- (S5) Arulsamy, N.; Bohle, D. S.; Butt, J. A.; Irvine, G. J.; Jordan, P. A.; Sagan, E. *J. Am. Chem. Soc.* **1999**, *121*, 7115-7123.